Light scattering by horizontally oriented ice plates. I. Scattering light intensity

A.V. Burnashov and A.G. Borovoy

Institute of Atmospheric Optics, Siberian Branch of the Russian Academy of Sciences, Tomsk

Received February 22, 2007

Light scattering phase functions on the horizontally oriented hexagonal ice plates are numerically calculated in the geometrical optics approximation. The main quantity indicators of halos (Sundog, parhelion of 120°, and others) are obtained at different light incidence angles and aspect ratios of the plate. The scattering phase function parameterization in parhelic and subparhelic circles is offered based on the integral contribution of narrow angular peaks (halos), based on the tabulated weight coefficients.

Introduction

Light scattering matrix for ice crystals in case of their random orientation was thoroughly investigated during the last 20–30 years by numerical methods. The obtained results were published, for example, in Refs. 1–4. It is known that ice crystals, when falling, often take a horizontal orientation due to the aerodynamic forces. It is confirmed by the fact that many well-known halo phenomena observed in the atmosphere, could arise only from the horizontal orientation of ice crystals. Remind that the atmospheric halos represent narrow stripes with bright spots in the sky, which are observed, when sunlight is passing through the crystal clouds.

According to the scattering theory, the scattered light intensity or its standardized value, the so-called scattering phase function, becomes the two-dimensional function, which is set on the sphere of scattering directions for the predominantly oriented non-spherical particles unlike the random orientation. The shape of the phase function also depends on direction of light incidence on the particle.

Thus, the halo patterns observed in the sky correspond to the scattering phase functions for the predominantly oriented ice crystals. These phase functions differ from zero only along some lines or stripes on the sphere of scattering directions.

The position and shape of halo stripes are well studied and explained within the framework of geometrical optics.[5] However, both the intensity and light polarization along these stripes, i.e., required radiation characteristics of crystal clouds, are not studied yet. The scattering phase functions for the horizontally oriented hexagonal plates and bars were calculated in Refs. 6 and 7, devoted to the given problem.

Indeed, a number of input parameters[6,7] is so insignificant that these data cannot be used for the more or less representative calculations of light scattering in crystal clouds. Besides, note that narrow sharp peaks are typical for the scattering phase functions calculated in the geometrical optics approximation. These peaks represent the integrated singularities, i.e., the phase function becomes infinite, but its integral remains finite by scattering directions. Therefore, it is impossible to restore the numerical values, necessary for calculating the problems of light multiple scattering from the scattering phase function diagrams presented in Refs. 6 and 7.

The scattering phase functions are calculated in the given study for a simpler case of the horizontally oriented hexagonal plates. These phase functions depend both on the shape parameter equal to the ratio of the plate's height to its diameter and on the light incidence angle. The main purpose of the calculations is to build the database, which can be used both for theoretical calculations of light transfer in the cirrus clouds and for the quantitative interpretation of halo patterns observed in the atmosphere. The scattering phase functions are calculated in the geometrical optics approximation according to the tracing algorithm of crystal faces.[8,9] These phase functions represent the histograms with a standard step of 1°. Tables 1, 2, and 3 present the interval of variation incidence angles of 10°, which is sufficient for numerical calculations of the atmospheric optics problems.

To avoid difficulties connected with sharp peaks in the scattering phase function, we separate all the peaks as single terms. Evidently, each peak is formed by the definite type of the photon path in a crystal and reflects some simple physical regularity. Hence, one must conclude that the shape of these peaks poorly depends both on light incidence angles and shape parameter of particles. It is possible to parameterize the scattering phase functions only by integrals of the peaks, which are called the weight coefficients in the given study. They determine the each peak contribution to the total scattering phase function, are tabulated as functions of light incidence angles and the crystal shape parameter.

Note that particles in the real atmosphere are not horizontally oriented, but oscillate relative to the horizontal plane. Therefore, the obtained data are

0235-6880/07/07 534-09 $02.00

only the necessary initial base for future development of an optical model of cirrus clouds. The effect of ice crystal orientation oscillations on the light scattering matrix was considered in Ref. 10, but the obtained results are illustrative and cannot be used by other authors, for example, for the numerical calculations of light multiple scattering in cirrus clouds. The light scattering matrices[11,12] on the predominantly oriented ice crystals are considered in detail, but the consideration is limited only by the light backscattering usable in the lidar sensing

1. Zenith distribution of scattered light

The hexagonal plate is one of the most distributed forms of ice crystals in crystal clouds. Besides, such plates represent the simplest shape of ice crystals. They represent a classical object for theoretical calculations. In the given work, we deal only with hexagonal plates, although some results will be applicable to the plates of more complicated shapes. The hexagonal plate is determined by two parameters: the side of hexagonal faces a and the distance between these faces L.

The scattering phase function in the geometrical optics approximation depends not on the absolute crystal sizes, but only on its shape, which is determined by the ratios of the plate height to the hexagon diameter $F = L/2a$. We will call F the shape parameter. If the main crystal axis passing through the centre of hexagonal faces is perpendicular to the horizon, such orientation is called horizontal. The fixed orientation of the plate is determined by the azimuth turn angle φ_0 relative to the principal axis. Further, the plate will be considered the randomly oriented in the horizontal plane, i.e., angular distribution of φ_0 in the interval $[0, 2\pi]$ is uniform. Then, the procedure of statistical averaging is reduced to the integral calculation

$$< \ldots > = \int_0^{2\pi} \ldots \mathrm{d}\varphi_0 / 2\pi.$$

Unlike the standard problem of light scattering on the sphere or on the non-spherical but randomly oriented particle, the scattering and extinction cross-sections for the non-spherical particle with the predominant orientation already depend on the light incidence direction. In the geometrical optics approximation, the extinction cross section is equal to the particle projection area relative to the light incidence direction, and then this area is averaged over φ_0. In particular, for the hexagonal plate randomly oriented in the horizontal plane, the extinction cross section is described by the following formula:

$$<S> = S_1 \cos\theta_0 + 3S_2 \sin\theta_0 \, <|\cos\varphi_0|> = \\ = \frac{3\sqrt{3}}{2} a^2 \cos\theta_0 + \frac{6}{\pi} aL \sin\theta_0, \qquad (1)$$

where θ_0 is the angle between the principle axis of the plate and the light incidence direction; S_1 and S_2 are the areas of hexagonal and rectangular faces. In the visible wavelength range, light is not absorbed by ice, then the scattering cross section is also determined by the formula (1).

Parameter $<S>$ determines the averaged energy flow falling on the particle, which then is propagated in scattering directions. The distribution density of this energy flow in the scattering directions $\mathbf{n}$ will be called the scattered light intensity $I(\mathbf{n}, \mathbf{n_0})$, i.e.,

$$\int I(\mathbf{n},\mathbf{n}_0)\mathrm{d}\mathbf{n} = <S(\mathbf{n}_0)>,$$

where $\mathbf{n_0}$ is the incidence direction. The normalized scattered light intensity

$$p(\mathbf{n},\mathbf{n}_0) = I(\mathbf{n},\mathbf{n}_0) / <S(\mathbf{n}_0)>$$

is called the scattering phase function, where

$$\int p(\mathbf{n},\mathbf{n}_0)\mathrm{d}\mathbf{n} = 1.$$

Thus, the scattering phase function does not depend on the particle absolute sizes, but depends on $F = L/2a$. Besides, it depends on the incident light polarization, however, only the nonpolarized incident light will be considered in this work.

The scattering direction $\mathbf{n}$ is set by the zenith θ and azimuth φ angles of the spherical coordinate system. It is convenient to designate the down-going vertical as $\theta = 0$. For example, the sunrays follow this direction, when the Sun is at zenith. Due to the symmetry of plates relative to the horizontal plane, $0 \le \theta_0 \le \pi/2$ and $0 \le \theta \le \pi$. The azimuth scattering angle φ is counted off from the incidence direction azimuth. Note that when the sunlight passes through the crystal clouds, the observer on the Earth can see the light scattering in the forward hemisphere of the scattering $0 \le \theta \le \pi/2$, and from the airplane or from space, one can see only the back hemisphere $\pi/2 \le \theta \le \pi$.

The typical feature of the field scattered on the horizontally oriented plates, is the scattered light localization in four horizontal circles with zenith angles $\theta_j(\theta_0)$, where j equals to 1, ..., 4. In particular, when observing the scattered sunlight at the Sun altitude θ_0 the zenith angle of the first circle is equal to the incidence angle $\theta_1 = \theta_0$.

Since it passes through the Sun on the sphere of scattering directions, it is called the parhelic circle. The second circle θ_2 is also located in the forward hemisphere and has two different names. If it is located under the parhelic circle relative to the observer on the Earth, it is called the near-horizontal, and if above — the near-zenith. The third and the fourth circles $\theta_{3,4}$, observed from space, are formed symmetrically relative to the horizon: $\theta_{3,4} = \pi - \theta_{1,2}$. They are called the subparhelic and subnear-horizontal or subnear-zenith circles, respectively.

Describe the formation of these circles in the geometrical optics approximation. For the better interpretation, let us treat light as population of photons, where the radiation wave nature is ignored, and the photon is treated as a corpuscle linearly propagating in the uniform space. This treatment of radiation is widely used, for example, in problems described by the radiation transfer equations.[13] First, consider the light incidence on the flat medium boundary vertical relative to the Earth surface. As is known, the vertical component of photon velocity does not change when reflecting and refracting on such a plane, and the horizontal component is constant by module and only changes its direction depending on the plane orientation.

Therefore, when rotating the plane around the vertical axis, the reflected photons have the propagation directions, enclosed in a cone, whose aperture angle $\theta_1 = \theta_0$ corresponds to the angle of beam reflection from the vertical plane presented in Fig. 1*a*. From the opposite side of the rotating plane, the refracted photons also form a cone, but with different aperture angle. For the plates randomly oriented in the horizontal plane, the photon propagation directions inside the particles are concentrated in two cones corresponding to the entering of photons either through the horizontal or vertical faces. Then, a random number of collisions with any faces inside the crystal do not remove the photon out of its direction cone. As a result, the problem of zenith scattering angles is reduced to the plane problem of light reflection and transmission through the rectangular plate (see Fig. 1*a*) independently of the number of photon collisions.

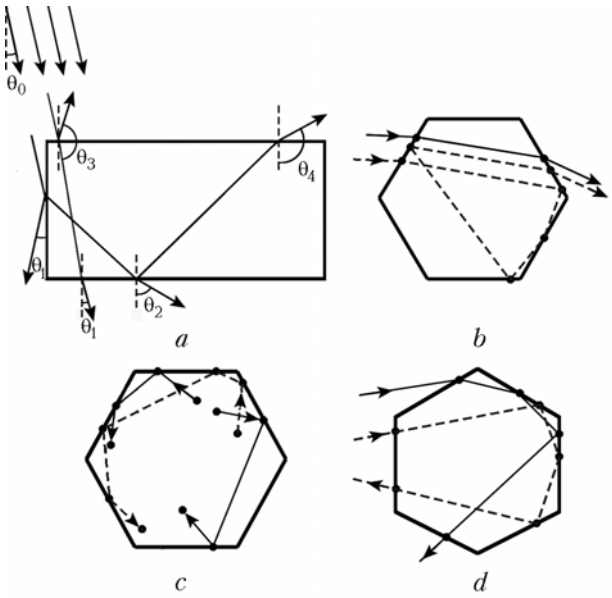

Fig. 1. The photon paths in the horizontally oriented hexagonal plate: *a* denotes the formation of four zenith scattering angles; *b* denotes the Sundog; *c* denotes the parhelion of 120°; *d* denotes the peak of 150°; *b*–*d* denote the light azimuth distributions in parhelic and subparhelic circles; the solid lines denote the main paths and the dashed lines denote the accompanied paths.

As it follows from Fig. 1*a*, the photons falling on the upper horizontal face and leaving after the random number of collisions out of any horizontal face, form the parhelic ($\theta_1 = \theta_0$) and subparhelic ($\theta_3 = \pi - \theta_0$) circles. This is also valid for the photons falling on the vertical face and leaving from the vertical faces. If light falls on the horizontal face and leaves from the vertical face or, vice versa, then, due to the light transmission through the rectangular wedge with the refractive index n, the circles $\theta_2(\theta_0)$ and $\theta_4(\theta_0)$ are obtained.

Consider θ_2 positions from the point of view of the observer from the Earth. Figure 1*a* presents the Sun falling counter-clockwise from zenith $\theta_0 = 0°$. In the beginning, when $\theta_0 = 0$, the rays sliding along the left vertical face, form, refracting through the left lower angle, the circle at the angle $\theta_2(0°) = \theta^*$, determined by the expression $\sin\theta^* = \sqrt{n^2 - 1}$, where n is the refractive index of the crystal. In particular, at $n = 1.31$ $\theta^* \approx 58°$. When the Sun descends down to the altitude $\theta_0 = \pi/2 - \theta^*$, then θ_2 descends to the horizon $\theta = \pi/2$, according to the formula

$$\theta_2(\theta_0) = \arcsin\sqrt{n^2 - \cos^2\theta_0} \qquad (2)$$

and is called the near-horizon. Note that $\theta_2(\pi/2 - \theta^*) = \pi/2$ due to the total internal reflection at the lower horizontal face, the light intensity in this circle becomes zero.

Figure 1*a* shows that the right upper angle does not form the refracted beam due to the total internal reflection on the right part of the face. Therefore, in the interval of incidence angles $\pi/2 - \theta^* < \theta_0 < \theta^*$, the second circle θ_2 does not appear owing to the total internal reflection. However, when θ_0 is equal to θ^*, the right upper angle begins to transmit the refracted light, and θ_2 appears at $\theta = 0$. Then, as far as the Sun descends, the near-zenith circle descends down to the critical angle $\theta_2(\pi/2) = \pi/2 - \theta^*$, observed at sunset. The dependence of the scattering angle on the incidence angle is described by the inverse function to Eq. (2). The circle $\theta_4(\theta_0)$ is symmetrical relative to the horizontal plane.

Hence, the emergence of four circles in the scattered light is induced by the horizontal and vertical faces in crystals and does not depend on the shape of the horizontally oriented plates. Thus, the specified four circles are characteristic for the horizontally oriented plates of any shape. Strictly speaking, the shape of the plates should be convex. If the plates have the form of stars, the photons going out of one end of the star at angles of θ_2 and θ_4, can go into another end of the star. In this case, this will lead to the emergence of additional circles or scattering angles. Our estimations show that one can neglect these components due to their insignificant energy. Besides, at $\theta^* > \theta_0 > \pi/2 - \theta^*$, when the scattering occurs only at $\theta_1 = \theta_0$ and $\theta_3 = \pi - \theta_0$, the additional scattering angles cannot appear in general for the plates of any shape.

Thus, the scattering phase function for the horizontally oriented plates consists of four functions localized on the circles θ_j:

$$p(\mathbf{n},\mathbf{n}_0) = \sum_{j=1}^{4} \delta(\mathbf{n} - \mathbf{n}_j) P_j(\varphi), \qquad (3)$$

where the δ-function denotes the localization of functions on the circle, and the functions of azimuth scattering angle $P_j(\varphi)$ have the meaning of scattering phase function of the given circle. A normalization condition of the total scattering phase function by a unit leads to the normalization of functions $P_j(\varphi)$ by the following coefficients:

$$Q_j(\theta_0, F) = \int_0^{2\pi} P_j(\varphi) \mathrm{d}\varphi, \qquad (4)$$

where

$$\sum_{j=1}^{4} Q_j = 1.$$

The coefficients Q_j have the physical meaning of weight coefficients at energy distribution of the scattered field in these four circles.

Table 1 presents the calculated coefficients Q_i for three values of F: 0.1, 0.2, and 0.4 at different incidence angles. The refractive index of ice is equal to 1.31.

Table 1. Scattered light distribution in four zenith circles at different light incidence angles for *F* equal to 0.1, 0.2, and 0.4, respectively. Total energy is under 100% due to the ignoring of paths with the number of photon internal collisions more than 6

Weight coefficient, %	Incidence angle θ_0, degrees							
	10	20	30	40	50	60	70	80
	$F = 0.1$							
Q_1	95.2	92.8	90.4	86.5	86.7	80.2	64.1	35.5
Q_2	1.4	3.7	5.8	0	0	1.2	3.9	3.5
Q_3	3.4	3.4	3.7	4.7	10.3	16.1	29.7	58.6
Q_4	<0.1	<0.1	<0.1	0	0	<0.1	<0.1	<0.1
In total	100	99.9	99.9	91.2	97	97.5	97.7	97.6
	$F = 0.2$							
Q_1	93.8	89.6	86.5	82	84.5	77.7	47.5	44.5
Q_2	2.6	7.1	8.6	0	0	2	5.9	5.5
Q_3	3.5	3.2	4.7	12.6	12.3	17.5	43.7	47.9
Q_4	<0.1	<0.1	<0.1	0	0	<0.1	<0.1	<0.1
In total	99.9	99.9	99.8	94.6	96.9	97.2	97.1	97.9
	$F = 0.4$							
Q_1	91.8	84.4	75.4	82.2	67.4	54.2	53	64.3
Q_2	4.9	12.8	16	0	0	3.1	8.1	6
Q_3	3.1	2.7	5.2	13	28.6	40.4	37	27.4
Q_4	<0.1	<0.1	<0.1	0	0	<0.1	<0.1	<0.1
In total	99.8	99.9	99.6	95.2	96	97.7	98.1	97.7

The main part of the scattered energy (70–90%) is concentrated in the first (parhelic) circle θ_1. The circle θ_4 contains no more than 0.1% of the scattered energy and is of no practical interest. The rest two circles θ_2 and θ_3 redistribute no more than 30% of the energy, and here the energy redistribution is connected with appearance or disappearance of total internal reflection when passing the right angle (see Fig. 1*a*).

2. Azimuth distribution of scattered light

The scattered field goes out of crystal faces in the form of plane-parallel beams with cross section in the form of polygons. These beams are propagated into different scattering angles and have a different polarization. Each beam is characterized by its photon path, i.e., by the sequence of photon collisions with definite crystal faces. We have developed a program,[8,9] which allows calculating all the outgoing beam parameters for the time no more than 1 min at a fixed orientation of the crystal. For the horizontally oriented plates, all beams on the sphere of scattering directions correspond to the points at four above-mentioned circles, where each point is described analytically by the Dirac δ-function. The scattered light intensity along the circle at a fixed orientation of the plate is described by the expression

$$I(\varphi) = \sum_k s_k(\varphi_0) N_k(\varphi_0) \delta[\varphi - \varphi_k(\varphi_0)], \qquad (5)$$

where the index j, indicating the circle number, is missed for briefness; the index k corresponds to a definite photon path, so that summation is carried out by all paths, i.e., beams; the function $\varphi_k(\varphi_0)$ describes the azimuth direction of the k-beam propagation at azimuth angle φ_0 of plate orientation; N_k is the ray intensity in the k-beam, which is calculated with regard for polarization at the given angles of the photon reflection and refraction by the crystal faces in correspondence with the Fresnel coefficients; s_k is the cross section area of the k-th beam. The average scattered radiation intensity by the plate orientations is easily calculated due to the δ-function in Eq. (5)

$$<I(\varphi)>= \sum_k s_k(\varphi) N_k(\varphi) \left(\frac{\mathrm{d}\varphi_0}{\mathrm{d}\varphi_k} \right). \qquad (6)$$

The last term in Eq. (6) is equal to the derivative of $\varphi_0(\varphi_k)$, inverse to $\varphi_k(\varphi_0)$. Equation (6) is convenient for analytical consideration, and at numerical calculations, we calculate directly the intensity histograms along the circles with averaging over φ_0 and obtain the scattering phase functions for the j-th circle by the formula

$$P_j(\varphi) = <I_j(\varphi)> / <S> . \qquad (7)$$

Henceforth, the scattering phase functions P_j are divided into sums of a small number of terms

$$P_j(\varphi) = \sum_m P_{jm}(\varphi),$$

where

$$\int_0^{2\pi} P_{jm}(\varphi)\mathrm{d}\varphi = Q_j c_{jm}; \quad \sum_m c_{jm} = 1. \qquad (8)$$

Here the coefficients c_{jm} have a physical meaning of weight coefficients determining a fraction of energy inside the given j-circle falling on the m-term. The functions $P_{jm}(\varphi)$ will be called the scattering phase functions for the given term.

3. The first (parhelic) circle

The main part of the scattered light energy is concentrated in the parhelic circle. Figure 2 presents the scattering phase functions in the parhelic circle $P_1(\varphi)$ for the plate with $F = 0.2$ at different incidence angles. Here, at small $\theta_0 = 15°$ (Fig. 2*a*), the light falling on the upper hexagonal face is predominant.

On the contrary, at $\theta_0 = 75°$ (Fig. 2*c*), the light falling on the vertical faces prevails. Figure 2*b* presents the intermediate case ($\theta_0 = 45°$). The numerical results in Fig. 2 represent histograms calculated at a standard step of 1°. The number of photon collisions was limited by 7, since no more than 2% of the scattered energy falls on the highest orders of collisions.

As it follows from Fig. 2, four peaks are significant in the azimuth scattering phase functions $P_1(\varphi)$, we separate them in individual terms of expansion (8): a peak in forward direction ($m = 1$), the Sundog ($m = 2$), the parhelion of 120° ($m = 3$), and a peak of 150° ($m = 4$). Other photon paths form more or less smooth φ dependence and are united into the remainder ($m = 5$).

Let us path to the qualitative description of these terms. As follows from the results of the numerical calculation, each peak is formed by a small number of definite paths. The angular dependence for each term of expansion (8) reflects a simple physical regularity and slightly depends on shape parameters of the crystal and the light incidence angle. The main dependence of azimuth scattering phase functions on the incidence angles and shape parameters is manifested itself only in values of weight coefficients c_{jm}. This important conclusion allows parameterization of the scattering phase functions by c_{jm} values, which are presented in Tables 2 and 3.

In particular, any two parallel faces of a crystal are equivalent to the plane-parallel plate. Therefore, the photon passed through these faces during two collisions, leaves the crystal in a strictly forward scattering direction. The angular distribution of the photons is described by the Dirac δ-function. The same is valid for photons, which are multiply rereflected from these faces. As a result, we obtain the peak in the forward direction $P_{11}(\varphi) = Q_1 c_{11}\delta(\varphi)$, whose angular distribution is described by the Dirac δ-function, and the calculated weight coefficients c_{11} are presented in Table 2 in the column "forward peak."

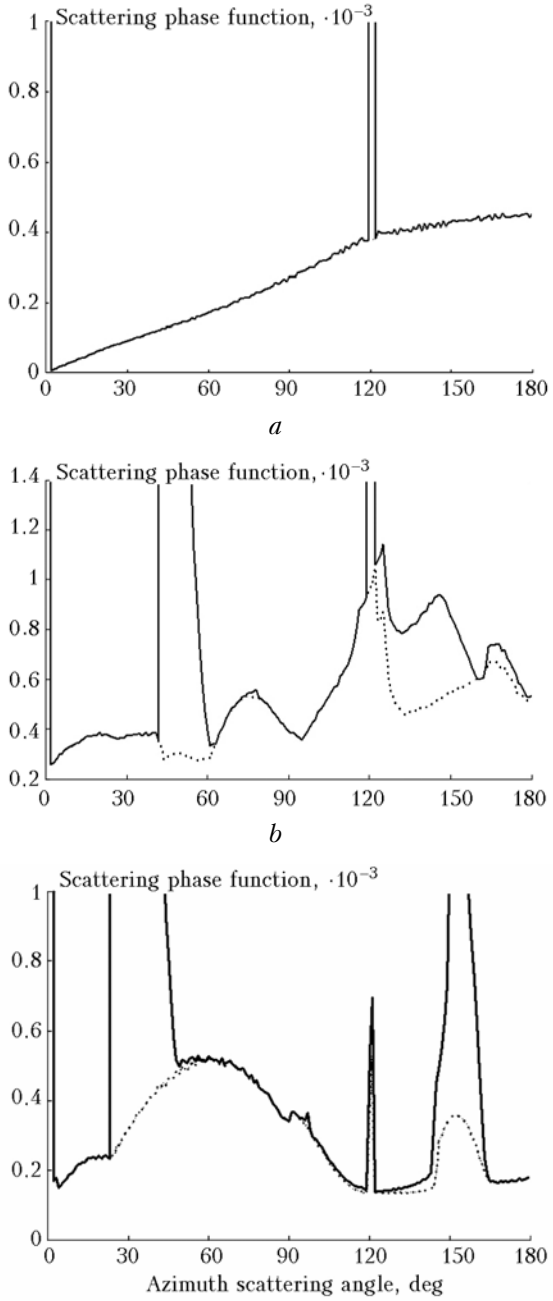

Fig. 2. Azimuth scattering phase functions in the parhelic circle for the plate with $F = 0.2$ at light incidence angles $\theta_0 = 15°$ (*a*), 45° (*b*), and 75° (*c*).

The next peak ($m = 2$) is called parhelion (or the Sundog). The Sundog is formed due to the photon passage through the wedge at $\gamma = 60°$, formed by the rectangular faces of the plate (see Fig. 1*b*). In a general case,[14] the passage of photons through the wedge with a random γ and their random incidence direction is described by quite simple analytical expressions. According to these expressions, the longitudinal component of the photon propagation direction does not change after passing through the wedge.

Table 2. Weight coefficients c_{1m} of peaks in the parhelic circle for the plates with $F = 0.1$, 0.2, and 0.4

Weight coefficient, %	Incidence angle θ_0, degrees								
	10	20	30	40	50	60	70	80	90
					$F = 0.1$				
c_{11} (forward peak)	96.8	94.8	92.8	90.1	83.6	83.4	83.5	74.8	35.6
c_{12} (Sundog)	0	0	0	0.7	2.7	4.6	5.4	13.2	49.7
c_{13} (parhelion of 120°)	<0.1	<0.1	0.1	0.1	0.1	0.2	0.3	0.3	<0.1
c_{14} (peak of 150°)	0	0	0	0	0	<0.1	0.1	0.3	2.7
c_{15} (remainder)	3.1	5.1	7	9	13.5	11.7	10.6	11.3	11.9
					$F = 0.2$				
c_{11} (forward peak)	94	89.8	86.1	80.7	72.9	70.7	71.4	46.3	35.6
c_{12} (Sundog)	0	0	<0.1	2.3	7.8	10.2	5.2	34.5	49.7
c_{13} (parhelion of 120°)	<0.1	0.1	0.2	0.4	0.5	0.7	1.2	0.7	<0.1
c_{14} (peak of 150°)	0	0	0	0	<0.1	<0.1	0.6	1.4	2.7
c_{15} (remainder)	5.9	10	13.6	16.5	18.7	18.3	21.5	17	11.9
					$F = 0.4$				
c_{11} (forward peak)	88.4	79.6	72.3	69.1	48.2	33.4	28	28.8	35.6
c_{12} (Sundog)	0	0	0.1	1.3	3.8	14.9	32.4	48.4	49.7
c_{13} (parhelion of 120°)	<0.1	0.3	0.9	1.2	2.4	3.5	3.3	1	<0.1
c_{14} (peak of 150°)	0.0	0	0	0.2	1.1	1.8	3.7	3.5	2.7
c_{15} (remainder)	11.5	20	26.6	28.1	44.5	46.2	32.1	17.3	11.9

A perpendicular component is found from the plane problem of photon passage through the wedge, but the refractive index inside the wedge n is substituted with the efficient refractive Bravais index $n' = (n^2 - \cos^2\beta)^{1/2}/\sin\beta$, where β is the angle between the photon incidence direction and the wedge rib. If to rotate the wedge around its rib, the maximal deviation of the emitted photons' direction is observed at their tangent incidence on the wedge's face. This maximal azimuth angle deviation is described by the following formula:

$$\varphi_{\max} = \gamma + \arcsin\left(\cos\gamma - \sqrt{n^2 - 1}\,\frac{\sin\gamma}{\sin\beta}\right) - 90^\circ =$$

$$= -30^\circ + \arcsin\left(\frac{1}{2} - \sqrt{n^2 - 1}\,\frac{\sqrt{3}}{2\sin\beta}\right). \qquad (9)$$

As far as the wedge rotates, the photon deviation is firstly decreased up to attaining the minimal value of azimuth angle described by the formula:

$$\varphi_{\min} = \gamma + 2\arcsin\left(-n'\sin\frac{\gamma}{2}\right) = 60^\circ + 2\arcsin(-n'/2). \qquad (10)$$

Note that at $\varphi = \varphi_{\min}$, the photon path cuts off equal segments of both wedge faces. Then, the photon deviation increases again. Figure 1*b* presents the path contributing to the interval of azimuth angles determined by Eqs. (9) and (10). In Eq. (6), at minimal deviation angle, we have $d\varphi_k/d\varphi_0 = 0$. Since $d\varphi_0/d\varphi_k = \infty$, the averaged intensity of the scattered light at the minimal deviation becomes infinity, i.e., it is an integrated singularity. This is the very bright spot, which is perceived by the observer as a Sundog when the sunlight passes through the crystal clouds.

In spite of a series of statements, which can be found in publications, the integrated singularities in scattering phase functions do not break any physical principles, since the experimentally registered values are not the scattering phase functions themselves, but their integrals in some finite angular limit corresponding to the viewing field angle of the receiving equipment. Figure 3 presents the calculated scattering phase functions at different incidence angles.

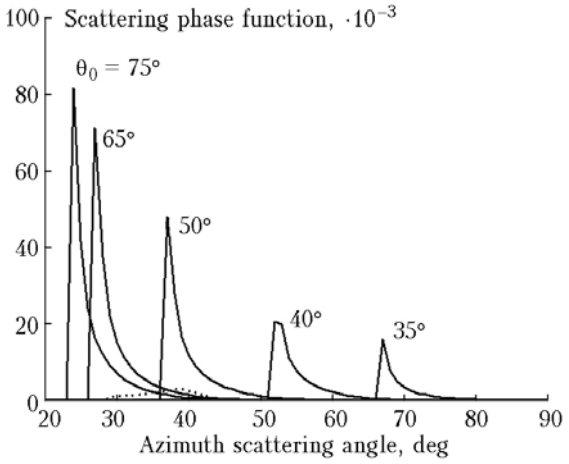

Fig. 3. Scattering phase functions of the Sundog $P_{12}(\varphi)$ at different incidence angles. Solid lines correspond to the main path, and the dashed line shows the scattering phase function for the accompanied path (multiplied by 100) at a zenith incidence angle of 75°.

Remind that the calculated phase functions represent histograms with a step of 1°, which leads to the finite intensity value at the left boundary of the interval. As is seen, the Sundog brightness is maximal at sunrise or sunset.

Under Sundog, we mean not only the intensity singularity at the left edge, but the whole phase function presented in Fig. 3. Just this function forms

the Sundog peak in a total scattering phase function in Fig. 2.

Note that the number of collisions in photon paths forming the Sundog peak can be random, since the additional photon collision with crystal's hexagonal faces does not change the path projection on the horizontal plane presented in Fig. 1*b*.

The numerical calculations have shown that accompanied photon path, presented in Fig. 1*b* by the dashed line, makes an essential contribution to the right edge of the Sundog peak. Figure 3 presents the accompanied path phase function for the single incidence angle by dashed lines. The term "Sundog" combines both types of paths. Table 2 presents the Sundog weight coefficients c_{12}.

The third peak $m = 3$ in the scattering azimuth phase function is described analytically, like the first peak, by the Dirac δ-function: $P_{13}(\varphi) = Q_1 c_{13} \delta(\varphi - 120°)$, and called the parhelion of 120°. The appearance of this peak can be easily explained if to consider the auxiliary plane problem of photon reflection inside the random polygon. Let the photon with random incidence direction be reflected from two faces with an angle γ between them as shown in Fig. 1*c*. The photon deviation in this cease does not depend on turn of the polygon and is equal to $\varphi = 2(180° - \gamma)$.

For the case of hexagonal plate, the path is realized, when the photon goes into crystal through the top hexagonal face and goes out of crystal through the bottom hexagonal face after two collisions with vertical faces. Then, the paths shown in Fig. 1*c*, correspond to the horizontal component of the photon propagation direction. As a result, the paths form the fixed glowing point at an angle of 120° (and at symmetrical angle of 240°) when turning the plate in the horizontal plane.

Apart from the main paths (see Fig. 1*c*, solid line), two types of the accompanied paths contribute to the parhelion of 120°. One of them corresponds to the main path, but the number of collisions is increased here (see Fig. 1*c*, the dashed line). In the second type of the accompanied paths, light is transmitted through vertical faces. Since the contribution from the second type turned out to be essentially smaller than that of the first type, the second type of paths is not presented in Fig. 1. The weight coefficient c_{13} in Table 2 terms all these paths "parhelion of 120°."

The fourth peak $m = 4$ was not described earlier in the literature. It appears at large zenith angles near azimuth scattering angle of 150°. This peak is formed by the main and accompanied paths shown in Fig. 1*d*. Phase functions of these paths are presented in Fig. 4.

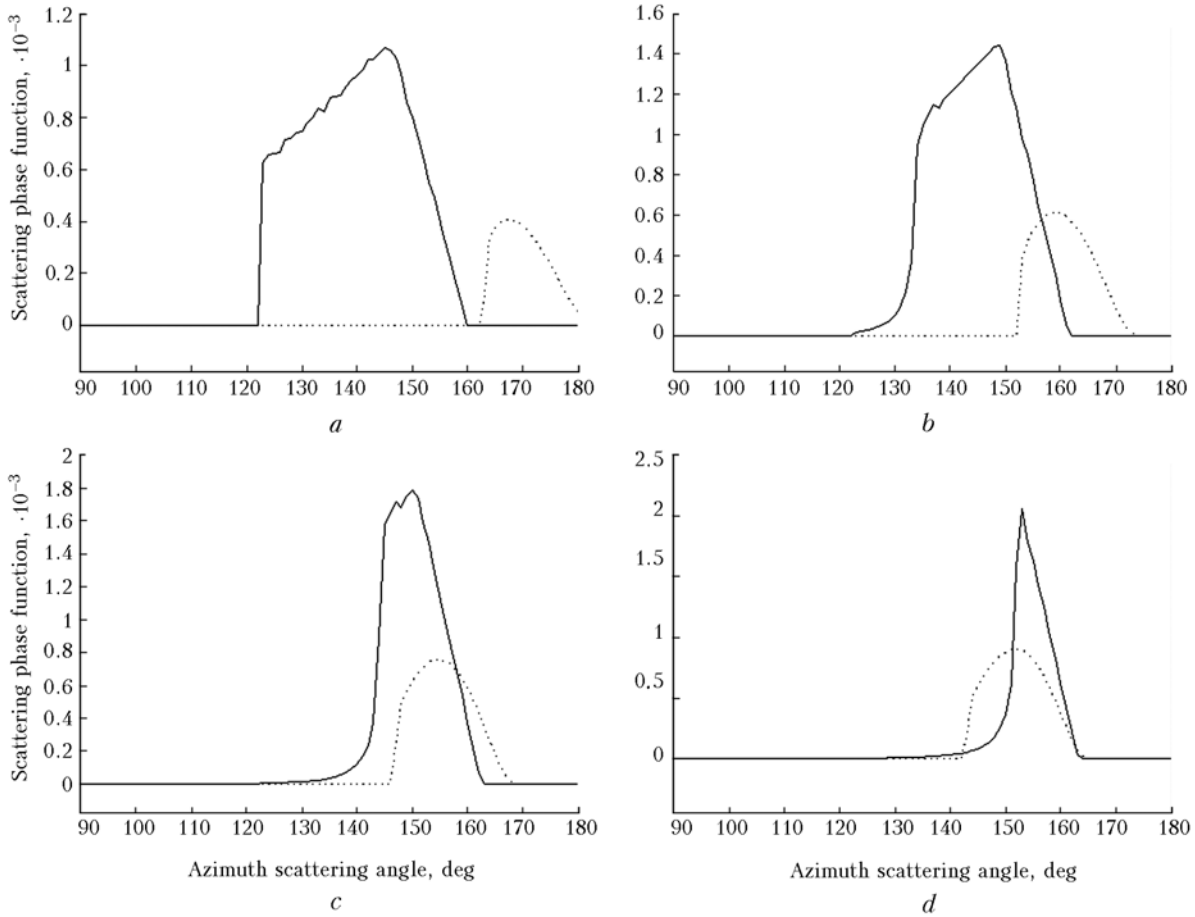

Fig. 4. Scattering phase functions $P_{14}(\varphi)$ of main (solid line) and accompanied (dashed line) paths forming a peak of 150° at different zenith incidence angles $\theta_0 = 45°$ (*a*), 55° (*b*), 65° (*c*), and 80° (*d*).

The appearance of a peak of 150° is accounted for the specific manifestation of the total internal reflection on paths with a greater number of photon collisions. Actually, let all the photon collisions with faces be carried out without total internal reflection for the given path. If at the crystal rotation on the path, there appears a total internal reflection from one of the faces, it is manifested itself as a sharp boundary, separating the regions with high and small intensities of the scattered light. Besides, there are scattering angle boundaries for each path induced by the geometry of particles, as we could see by the example of a Sundog. At photon collisions with a large number of faces, the integration of these boundaries leads to the narrow interval of angles, efficiently transmitting the radiation. Figure 4 demonstrates this regularity. The total weight coefficient c_{14} for the peak of 150° is presented in Table 2.

Thus, we distinguished all paths producing significant peaks in the total scattering phase function P_1, the remainder $m = 5$ is more or less smoothly varying function of φ that is shown in Fig. 2 by the dashed line. The weight coefficient for the remainder c_{15} is presented in Table 2.

4. The second (near-zenith/near-horizon) circle

The second circle located in the forward hemisphere of scattering directions is mainly formed by paths with two collisions, when the photons pass through the wedge at an angle of 90°. Here at the hexagonal plate rotation, the edge of the plate rotates in the horizontal plane. Therefore, the maximal light transmission by the wedge occurs when the wedge rib is perpendicular to the incidence direction. In this case, the azimuth photon deviation is equal to zero and the scattering phase function at $\varphi = 0$ is maximal. This regularity is demonstrated in Fig. 5.

For the near-horizon circle, such path begins from the vertical face; therefore, the maximal azimuth deviation of photons occurs at sliding incidence on the vertical face. Thus, the scattering phase function for such path differs from zero in the interval $[0°, \varphi_{max}]$, where for the right boundary of the interval, the following analytical expression can be obtained:

$$\varphi_{max} = \arctan(\sqrt{n^2 - 1}/\sin\theta_0). \qquad (11)$$

The same path for the near-zenith circle starts from the top hexagonal face. The right boundary of angular interval $[0°, \varphi_{max}]$ occurs due to the total internal reflection on the vertical face. In this case, it is easily to obtain the following expression:

$$\varphi_{max} = \arcsin(\sqrt{n^2 - 1}/\sin\theta_0). \qquad (12)$$

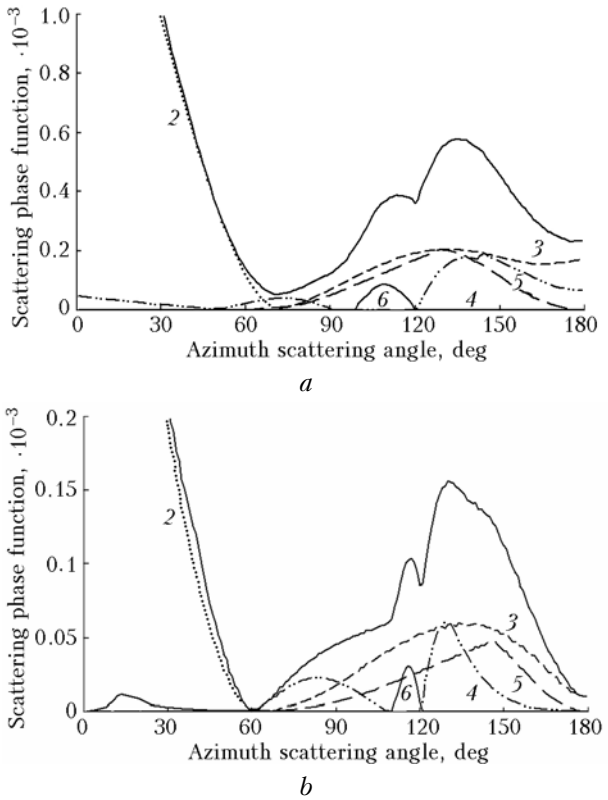

Fig. 5. Scattering phase functions $P_2(\varphi)$ for the near-horizon (*a*) and near-zenith (*b*) circles for incidence angles of 15 and 75°, respectively. The top line corresponds to the total scattering phase function, and the curve numbers specify the scattering phase functions of the given multiplicity of photon collisions.

Our calculations have shown that no more than 5% of energy falls on the path with a larger number of collisions in the second circle. Therefore, the contribution of these paths is of no practical interest from the point of view of integral parameters. As it follows from the scattering phase functions $P_2(\varphi)$ of the second circle, presented in Fig. 5, paths with a greater number of collisions fill, in general, the remaining interval of azimuth angles $\varphi > \varphi_{max}$. As compared to the first circle, the second one has no so sharp peaks in the scattering phase functions. The peaks appear only in small in magnitude terms, which correspond to the greater multiplicities of photon collisions. These peaks in the parhelic circle are accounted for transmission truncation due to the total internal reflection and path geometry.

5. The third (subparhelic) circle

The third circle appears in the back hemisphere of scattering directions at a zenith angle of $\theta_3 = \pi - \theta_0$. It is formed by the same photon paths as in the parhelic circle, but at additional reflection. Therefore, in the third circle, the same peaks as in the parhelic circle are observed. The calculated weight coefficients for the third circle are presented in Table 3.

Table 3. Weight coefficients c_{3m} of peaks in the subparhelic circle for the plates with $F = 0.1$, 0.2, and 0.4

Weight coefficient, %	Incidence angle θ_0, degrees							
	10	20	30	40	50	60	70	80
				$F = 0.1$				
c_{31} (forward peaks)	98.2	95.9	94.8	77.8	65.7	62.3	58.9	63.4
c_{32} (Sundog)	0	0	< 0.1	16.4	27.2	31.3	40.4	32.7
c_{33} (parhelion of 120°)	< 0.1	< 0.1	< 0.1	< 0.1	< 0.1	< 0.1	0.2	0.2
c_{34} (peak of 150°)	0	0	0	0	< 0.1	< 0.1	0.2	0.2
c_{35} (remainder)	1.8	4.1	5.2	5.8	7.1	6.4	0.3	3.5
				$F = 0.2$				
c_{31} (forward peaks)	96.4	93.2	91.4	76.9	70.7	42.4	50.1	58.8
c_{32} (Sundog)	0	0	< 0.1	19.1	22.1	40.2	42	31.8
c_{33} (parhelion of 120°)	< 0.1	< 0.1	< 0.1	< 0.1	0.2	0.4	0.7	0.5
c_{34} (пик 150°)	0	0	< 0.1	< 0.1	< 0.1	2.0	0.1	2.1
c_{35} (остаток)	3.6	6.8	8.6	4	7	15	7.1	6.8
				$F = 0.4$				
c_{31} (forward peaks)	93.3	81.3	74.5	66.8	48.9	48.2	47.7	53.2
c_{32} (Sundog)	0	0	10.5	17.9	44.7	40.4	38.7	31.3
c_{33} (parhelion of 120°)	< 0.1	< 0.1	< 0.1	0.5	0.4	0.7	1.7	1.8
c_{34} (peak of 150°)	0	< 0.1	< 0.1	0.4	0.7	3.7	3.2	5.1
c_{35} (remainder)	6.7	18.7	14.6	14.4	5.3	7	8.7	8.6

Note. At an incidence angle of 90°, the parhelic and subparhelic circles are merged; therefore, the weight coefficients of peaks are presented in Table 2.

The fourth circle bears no more than 0.1% of the scattered energy, therefore, it is beyond the practical interest.

Conclusion

When considering the scattering phase functions for the horizontally oriented hexagonal ice plates, the main attention is paid to those terms in the scattering phase function expansion (8) in the parhelic and subparhelic circles, which have a shape of narrow peaks (halos). Since the angular dependence of scattered radiation inside these peaks slightly depends on F of plates and light incidence angle, the scattering phase functions can be characterized only by the integral characteristics of these peaks. Such approach is justified, for example, when estimating the vertical radiation flows or when calculating the light multiple scattering, where the detailed angular distribution of scattered light has no principal importance. In other situations, when the scattered light measurements take place only at some fixed scattering angles, the given approach can be rough, in this case rather laborious calculations are required.

Acknowledgements

This work is supported in part by the Russian Foundation for Basic Research (Grants Nos. 05-05-39014 and 06-05-65141) and INTAS (Grant No. 05-1000008-8024).

References

1. O.A. Volkovitsky, L.N. Pavlova, and A.G. Petrushin, *Optical Properties of Crystal Clouds* (Gidrometeoizdat, Leningrad, 1984), 200 pp.
2. K.N. Liou, Y. Takano, and P. Yang, in: *Light Scattering by Nonspherical Particles: Theory, Measurements, and Applications* (Acad. Press, San Diego, 2000), pp. 417–449.
3. P. Yang and K.N. Liou, in: *Light Scattering Reviews* (Springer–Praxis, Chichester, 2006), pp. 31–71.
4. D.N. Romashov, Atmos. Oceanic Opt. **14**, No. 2, 102–110 (2001).
5. W. Tape, *Atmospheric Halos* (American Geophysical Union, Antarctic Res. Series, Washington, 1994), Vol. 64, 139 pp.
6. Y. Takano and K.N. Liou, J. Atmos. Sci. **46**, No. 1, 3–19 (1989).
7. Y. Takano and K.N. Liou, J. Opt. Soc. Am. A **10**, No. 6, 1243–1256 (1993).
8. A.G. Borovoy and I.A. Grishin, J. Opt. Soc. Am. A **20**, No. 11, 2071–2080 (2003).
9. A.G. Borovoy, N.V. Kustova, and U.G. Oppel, Opt. Eng. **44**, No. 7, 171–208 (2005).
10. V. Noel, G. Ledanois, H. Chepfer, and P.H. Flamont, Appl. Opt. **40**, No. 24, 4365–4375 (2001).
11. D.N. Romashov, B.V. Kaul, and I.V. Samokhvalov, Atmos. Oceanic Opt. **13**, No. 9, 794–800 (2000).
12. B.V. Kaul, I.V. Samokhvalov, and S.N. Volkov, Appl. Opt. **43**, No. 36, 6620–6628 (2004).
13. S. Chandrasekar, *Radiation Energy Transfer* (Izd. Inostr. Lit., Moscow, 1953), 430 pp.
14. W. Tape, J. Opt. Soc. Am. **70**, No. 10, 1175–1192 (1980).